Systems & Control Transactions

Research Article - Peer Reviewed Conference Proceeding
ESCAPE 35 - European Symposium on Computer Aided Process Engineering
Ghent, Belgium. 6-9 July 2025
Jan F.M. Van Impe, Grégoire Léonard, Satyajeet S. Bhonsale,
Monika E. Polańska, Filip Logist (Eds.)

PSE PRESS

Multi-objective Optimization of Steam Cracking Microgrid for Clean Olefins Production

Saba Ghasemi Naraghi, Tylee Kareck[a], and Zheyu Jiang[s]*

[a] Oklahoma State University, Department of Chemical Engineering, Stillwater, Oklahoma, USA
* Corresponding Author: zheyu.jiang@okstate.edu.

ABSTRACT

Olefins are essential precursors in producing a wide range of chemical products, including plastics, detergents, adhesives, rubber, and food packaging. Ethylene and propylene are the most ubiquitous olefin components and are predominantly produced through steam cracking. However, steam cracking is highly energy- and carbon-intensive, making its decarbonization a priority as the energy sector shifts toward clean, renewable electricity. Electrifying the steam cracking process is a promising pathway to reduce carbon emissions. However, this is challenged by the intrinsic conflict between the continuous operational nature of ethylene plants and the intermittent nature of renewable energy sources (e.g., solar and wind) in modern power systems. Massive energy storage systems or full plant reconfigurations to meet the power demand of electrified crackers are shown to be economically and practically infeasible. Thus, a more viable solution is to pursue a gradual electrification pathway and operate an ethylene plant as a microgrid that adopts diverse energy sources. To optimize the operational strategy of such a microgrid considering uncertainties in renewable energy generation and market prices, in this work, we introduce a stochastic multi-objective optimization approach that minimizes operating costs and carbon emissions of steam cracking. Results from a case study not only elucidate the trade-offs between economic and environmental objectives, but also provide insights into the optimal operating scheme in sustainable ethylene production.

Keywords: Steam cracking, Ethylene, Multi-objective Optimization, Renewable and Sustainable Energy, Decarbonization

INTRODUCTION

The U.S. energy landscape is undergoing a fundamental transition as the proportion of clean, renewable electricity in total U.S. electricity generation will double to 44% between now and 2050 [1]. Thus, electrification is a promising pathway to decarbonize various energy-intensive chemical processes, including the steam cracking process for olefins production. Recently, there have been significant advancements in electrified cracking technology [2]. While conventional cracking furnaces transfer only 40-45% of firing energy to process fluids, electrified furnaces achieve efficiencies of at least 95% [2-4]. Most U.S. ethylene plants are large-scale, continuously operating facilities with capacities exceeding 1 million tons annually. Due to the intermittent nature of variable renewable electricity (VRE), energy storage solutions must be in place. However, the intermittent nature and seasonal variation in VAE generation will lead to a 1~2-order increase in battery storage requirements compared to the storage requirement based on the average daily power supply, making energy storage purely using battery an expensive option [5,6]. On the other hand, the use of byproduct hydrogen (H_2) as energy storage substantially reduces battery size. The combined use of solar and wind energy can significantly reduce storage requirements [5]. And low but continuing use of fossil fuels and a gradual transition from conventional crackers to electrified ones are feasible intermediate solutions toward long-term complete decarbonization [7].

In **Figure 1**, we propose a novel process scheme for steam cracking decarbonization that incorporate these important aspects. The envisioned process is a microgrid – a localized electric grid capable of independent

operation. Both electrified and conventional crackers are considered in this superstructure. Diverse energy sources, including on-site VRE, battery storage, electrolyzers, H_2 fuel cells as well as conventional natural gas and liquid fuel, can be adopted. Operating the cracking plant as a microgrid offers several advantages, including enhanced resilience, efficiency, and flexibility [8]. For example, a microgrid can operate in grid-connected mode to benefit from low electricity prices or in islanded mode to ensure continuous operation during grid outages or price spikes.

This study builds on our previous work [7] and explores the optimization of microgrid scheduling for clean ethylene production based on the superstructure shown in **Figure 1**. A hypothetical ethylene plant located on the Texas Gulf Coast is used as a case study, with ethane selected as the primary feedstock due to its prevalence in U.S. crackers [1]. A deterministic, steady-state, multi-objective MILP model will be developed to determine the optimal electrification level for our hypothetical plant, and uncertainties in VRE generation and market price predictions will be considered as different scenarios.

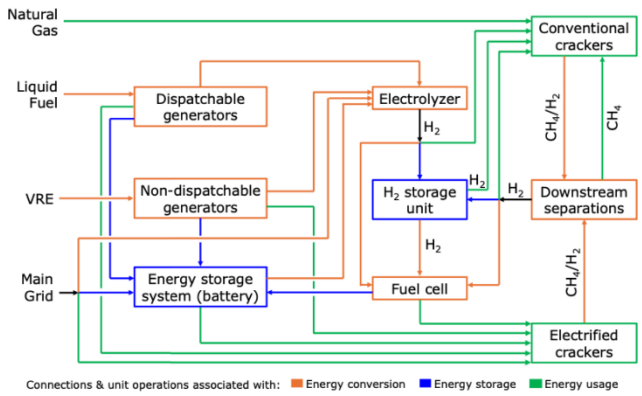

Figure 1. Our envisioned framework for using electricity to supply process heat for steam cracking [7]. Based on the context, the connections shown in the superstructure can represent either energy or mass flows.

MULTI-OBJECTIVE SCENARIO-BASED OPTIMAL SCHEDULING FORMULATION

Before formulating the microgrid scheduling problem, a preliminary calculation [6] demonstrates the importance of incorporating diverse energy sources and energy storage systems for electrified cracking. In the case of a plant with an ethylene production capacity of 1 million tons/year, even if one ignores seasonal variation, since VRE is accessible for only 30% of the day on average, around 70% of the daily energy demand – equivalent to 3,356 MWh – must be stored to ensure uninterrupted operation of electrified crackers. Relying solely on battery would require an excessive amount of battery storage units. For example, if all the electricity is stored using Tesla Megapack, each with 3.9 MWh of energy capacity and 40.7 m^3 of storage volume [12], the resulting battery volume would occupy a massive structure of 32.7 m × 32.7 m × 32.7 m. Furthermore, this storage requirement could increase by one to two orders of magnitude due to variations in daily and seasonal weather patterns [5]. These findings highlight the need for a hybrid energy landscape, as illustrated in **Figure 1**, which integrates both dispatchable and non-dispatchable generators. Dispatchable generators, powered by fossil fuel (e.g., diesel) and controlled by microgrid master controllers, are subject to operational constraints such as generation limits, ramping rates, and minimum on/off times [13]. In contrast, non-dispatchable generators are driven solely by the availability and capacity of VRE sources and operate independently. Motivated by these results, we develop a multi-objective scenario-based mixed-integer linear programming (MILP) model to identify the optimal schedule for the microgrid and the optimal degree of electrification for ethane cracking.

Mathematical Formulation

In this section, we describe MILP model in detail. First, the objective function (1) minimizes the expected daily operating cost, which includes fuel costs (c^{NG}), electricity costs from the main grid (c^G), local energy generation costs by dispatch units (c^D) and fuel cell units (c^{FC}), startup (c^D_{SU}) and shutdown costs (c^D_{SD}), and H_2 generation(c^{EL}) and storage (c^{HS}) costs across all scenarios $\omega \in \Omega$. The maximization function in the startup and shutdown costs in the objective function can be easily linearized. Constraint (2) adopts the ϵ-constraint approach for modeling the trade-off between operating costs and environmental impacts by ensuring that the expected total released CO_2-equivalent emissions in every hour generated by all cracker units do not exceed a specified level. Note that burning one ton of natural gas in conventional cracker releases approximately 2.95 (E^{NG}) tons of CO_2-equivalent emissions [14]. Meanwhile, based on current power generation technologies, each MWh of electricity from the power grid is associated with 0.434 (E^G) tons of CO_2-equivalent emissions [15]. Equations (3) and (4) are energy balance equations with respect to the amount of ethylene produced by conventional crackers (CC) and electrified (EC) ones, respectively. In our previous work [7], we developed a differential-algebraic equation (DAE) numerical model for ethane cracking based on detailed kinetics model [16] and solved the resulting dynamic optimization problem in pyomo.dae [17] to obtain that the minimum energy required to produce one ton of ethylene in a conventional cracker (P^{CC}) and electrified cracker (P^{EC}) are 4.27 MWh and 1.75 MWh, respectively (due to different thermal efficiencies). The RHS of Equations (3) and (4) uses the lower heating values of natural gas

(LHV^{NG}) (13.826 MWh/ton) and H_2 (LHV^{H_2}) (33.320 MWh/ton). Assuming year-round continuous and steady-state operation of CCs and ECs, Equation (5) ensures that the hourly production rate of ethylene ($F^{C_2H_4}$) of all CCs and ECs must be 114.155 ton/h to achieve an annual production target of 1 million tons. After steam cracking, the product stream undergoes a series of downstream processing steps to obtain individual product streams, including C_2H_4, C_3H_6, H_2, and other value-added hydrocarbons. For CH_4 produced by ECs and CCs, it will be directly recycled to power the CCs, as shown in Equation (6). For byproduct H_2, it can either be stored in H_2 storage (HS) units, or be used to power the CCs or produce electricity in fuel cell (FC) units [18], as described in Equation (7). The mole fractions of CH_4 (R^{Mix,CH_4}) and H_2 (R^{Mix,H_2}) in the product mixture are 0.469 and 0.531, respectively [7]. Furthermore, we assume CH_4 and H_2 recovery rates in downstream separation units to be 99.7% (r^{CH_4}) and 99% (r^{H_2}), respectively [7]. Next, given that the ratio of product flow rates between H_2 and C_2H_4 (R^{H_2}) is 0.149 as determined from the DAE model [7], equations (8-9) indicate that not all CH_4 and H_2 produced have to be recycled. Equation (10) limits the amount of H_2 in a HS unit to its storage capacity (HSC) which is 15 tons. Equations (11-12) are hydrogen balances around the HS unit and electrolyzer (EL). The energy balance for the electrolyzer is shown in Equation (13) using the NREL-validated PEM stack efficiency (η^{EL}) of 73.6% [19] and the theoretical electrolysis energy requirement ($\dot{Q}^{H_2}$) of 40 MWh/ton. Equation (14) indicates the current H_2 production capacity ($F_{EL}^{H_2}$) from the electrolyzer (0.6 ton/h). The fuel cell energy balance, generation limit, and power distribution constraints are formulated in Equations (15-17), where we assume a 65% fuel cell efficiency (η^{FC}) and a power generation capacity ($\bar{P}^{FC}$) of 1 MW. Equations (18-22) show power distribution associated with the local non-dispatchable, dispatchable, energy storage system (both charging and discharging), and main grid. In Equation (23), we set the allowable power withdrawal from the main grid to the microgrid to be at most 50 MW ($\bar{P}^{G}$). Additional constraints related to local dispatchable generation, ramping, up/downtime, energy storage charging/discharging, and power storage are described in [9] and also included in the model [7].

$$\min \sum_{\omega\in\Omega}\sum_{t\in T}\rho_\omega[c^{NG}F_{CC,t,\omega}^{NG}\Delta t+\sum_{g\in G}\big(c^{NG}F_{g,t,\omega}^{D}\Delta t+ c^{D}p_{g,t,\omega}^{D}+ c_{SU}^{D}\max\{0,x_{g,t,\omega}^{D}- x_{g,t-1,\omega}^{D}\}+ c_{SD}^{D}\max\{0,x_{g,t-1,\omega}^{D}- x_{g,t,\omega}^{D}\}\big)+c_{t,\omega}^{G}P_{t,\omega}^{G}+c^{FC}p_{t,\omega}^{FC}+ c^{EL}F_{EL,t,\omega}^{H_2}\Delta t+ c^{HS}M_{HS,t,\omega}^{H_2}\ ],(1)$$

$$\sum_{\omega\in\Omega}\rho_w\Delta t\left[E^{NG}\left(F_{CC,t,\omega}^{NG}+F_{sep,t,\omega}^{NG}+\sum_{g\in G}F_{g,t,\omega}^{D}\right)+E^{G}P_{t,\omega}^{G}\right]\le\epsilon,\forall t\in T,\ (2)$$

$$P^{CC}F_{CC,t,\omega}^{C_2H_4}=LHV^{NG}\big(F_{CC,t,\omega}^{NG}+F_{sep,t,\omega}^{CH_4}\big)+LHV^{H_2}\big(F_{sep,t,\omega}^{H_2}+F_{EL,CC,t,\omega}^{H_2}+F_{HS,CC,t,\omega}^{H_2}\big),\forall t\in T,\omega\in\Omega,(3)$$

$$P^{EC}F_{EC,t,\omega}^{C_2H_4}=\sum_{g\in G}p_{EC,g,t,\omega}^{D}+P_{EC,t,\omega}^{ND}+P_{EC,t,\omega}^{G}+P_{EC,t,\omega}^{ESS}+P_{EC,t,\omega}^{FC},\forall t\in T,\omega\in\Omega,(4)$$

$$F_{CC,t,\omega}^{C_2H_4}+F_{EC,t,\omega}^{C_2H_4}=F^{C_2H_4},\quad\forall t\in T,\omega\in\Omega\ (5)$$

$$F_{sep,CC,t,\omega}^{CH_4}=r^{CH_4}R^{Mix,CH_4}\big(F_{CC,sep,t,\omega}^{C_2H_4,H_2}+F_{EC,sep,t,\omega}^{C_2H_4,H_2}\big),\forall t\in T,\omega\in\Omega,(6)$$

$$F_{sep,CC,t,\omega}^{H_2}+F_{sep,HS,t,\omega}^{H_2}+F_{sep,FC,t,\omega}^{H_2}=r^{H_2}R^{Mix,H_2}\big(F_{CC,sep,t,\omega}^{C_2H_4,H_2}+F_{EC,sep,t,\omega}^{C_2H_4,H_2}\big),\forall t\in T,\omega\in\Omega,(7)$$

$$F_{CC,sep,t,\omega}^{C_2H_4,H_2}\le R^{H_2}F_{CC,t,\omega}^{C_2H_4},\forall t\in T,\omega\in\Omega,(8)$$

$$F_{EC,sep,t,\omega}^{C_2H_4,H_2}\le R^{H_2}F_{EC,t,\omega}^{C_2H_4},\forall t\in T,\omega\in\Omega,(9)$$

$$0\le M_{HS,t,\omega}^{H_2}\le HSC,\forall t\in T,\omega\in\Omega,(10)$$

$$M_{HS,t,\omega}^{H_2}=M_{HS,t-1,\omega}^{H_2}+\Delta t\big(F_{sep,HS,t,\omega}^{H_2}+F_{EL,HS,t,\omega}^{H_2}-F_{HS,FC,t,\omega}^{H_2}-F_{HS,CC,t,\omega}^{H_2}\big),\forall t\in T,\omega\in\Omega,(11)$$

$$F_{EL,t,\omega}^{H_2}=F_{EL,FC,t,\omega}^{H_2}+F_{EL,HS,t,\omega}^{H_2}+F_{EL,CC,t,\omega}^{H_2},\forall t\in T,\omega\in\Omega,(12)$$

$$F_{EL,t,\omega}^{H_2}=\frac{\eta^{EL}}{\dot{Q}^{H_2}}\left(\sum_{g\in G}p_{EL,g,t,\omega}^{D}+P_{EL,t,\omega}^{ND}+P_{EL,t,\omega}^{G}+P_{EL,t,\omega}^{ESS}\right),\forall t\in T,\omega\in\Omega,(13)$$

$$0\le F_{EL,t,\omega}^{H_2}\le F_{EL}^{H_2},\forall t\in T,\omega\in\Omega,(14)$$

$$p_{t,\omega}^{FC}=\eta^{FC}LHV^{H_2}\big(F_{HS,FC,t,\omega}^{H_2}+F_{EL,FC,t,\omega}^{H_2}+F_{sep,FC,t,\omega}^{H_2}\big)\Delta t,\forall t\in T,\omega\in\Omega,(15)$$

$$0\le p_{t,\omega}^{FC}\le\bar{P}^{FC}x_{t,\omega}^{FC},\forall t\in T,\omega\in\Omega,(16)$$

$$p_{t,\omega}^{FC}=p_{EC,t,\omega}^{FC}+p_{ESS,t,\omega}^{FC},\forall t\in T,\omega\in\Omega,(17)$$

$$P_{t,\omega}^{WT}+P_{t,\omega}^{PV}=p_{EC,t,\omega}^{ND}+p_{ESS,t,\omega}^{ND}+p_{EL,t,\omega}^{ND},\forall t\in T,\omega\in\Omega,(18)$$

$$P_{g,t,\omega}^{D}=p_{EC,g,t,\omega}^{D}+p_{ESS,g,t,\omega}^{D}+p_{EL,g,t,\omega}^{D},\forall g\in G,t\in T,\omega\in\Omega,(19)$$

$$P_{C,t,\omega}^{ESS}=\sum_{g\in G}p_{ESS,g,t,\omega}^{D}+p_{ESS,t,\omega}^{G}+p_{ESS,t,\omega}^{ND}+p_{ESS,t,\omega}^{FC},\forall t\in T,\omega\in\Omega,(20)$$

$$P_{DC,t,\omega}^{ESS}=P_{EC,t,\omega}^{ESS}+P_{EL,t,\omega}^{ESS},\forall t\in T,\omega\in\Omega,(21)$$

$$P_{t,\omega}^{G}=p_{EC,t,\omega}^{G}+p_{ESS,t,\omega}^{G}+p_{EL,t,\omega}^{G},\forall t\in T,\omega\in\Omega,(22)$$

$$0\le P_{t,\omega}^{G}\le\bar{P}^{G},\forall t\in T,\omega\in\Omega.(23)$$

ILLUSTRATIVE CASE STUDY

In this section, we illustrate the proposed multi-objective scenario-based MILP model in a case study of a hypothetical plant designed with an ethylene production capacity of 1 million tons per year. Each cracking furnace in the U.S. typically can produce 100,000 to 250,000 tons of ethylene per year. Based on this, we assume the plant operates with five ethane crackers, each with a production capacity of 200,000 tons of C_2H_4 per year. The microgrid is equipped with 20 natural gas-powered local generators with minimum (resp. maximum) capacity of 1 (resp. 5) MW, a minimum up/downtime of 3 hr, a ramp-up/down rate of 2.5 MW/h, and an operating cost of $33.4/MWh. The battery storage units have a total capacity of 20 MWh with 5 hours of minimum charging/discharging time. The minimum and maximum capacities of charging/discharging power are 0.8 and 4 MW, respectively. Our planning horizon is 24 hours.

Table 1: Probability of generated scenarios for LMP, wind power, and PV.

Scenario number used in Table 2	Probability of uncertain parameter (%)		
	LMP	WP	PV
1	64.50	14.48	4.86
2	2.92	1.52	60.31
3	3.26	64.91	15.81
4	1.29	6.18	32.96
5	28.03	13.91	16.06

Table 2: Probability of generated scenarios (after scenario reduction) for the microgrid problem after scenario reduction.

Combined scenario	Selected LMP scenario	Selected WP scenario	Selected PV scenario	Probability (%)
1	5	3	2	18.21
2	1	3	4	45.56
3	1	1	3	4.54
4	5	3	3	9.50
5	1	3	5	22.19

Electricity market prices, along with solar and wind energy generation, are inherently intermittent. To account for these uncertainties in our model, we generate five scenarios for each uncertain parameter using Monte Carlo simulations based on a log-normal distribution, ensuring that no negative parameter values are produced [7]. These scenarios are derived using publicly available data from the Texas grid (ERCOT) for August 2024. For locational marginal pricing (LMP), we select Bus TC-KO arbitrarily as a representative case without loss of generality. **Table 1** summarizes the probabilities of scenarios for each uncertain parameter. Note that the combination of these scenarios results in $5^3 = 125$ possible outcomes. To manage this complexity, we apply a scenario reduction technique to identify 5 representative combinations. This is achieved using a probability distance algorithm based on the Kantorovich distance [9] (see **Table 2**). **Figures 2 through 4** illustrate the mean and average values for electricity market prices, wind power, and solar power across the 5 representative scenarios synthesized.

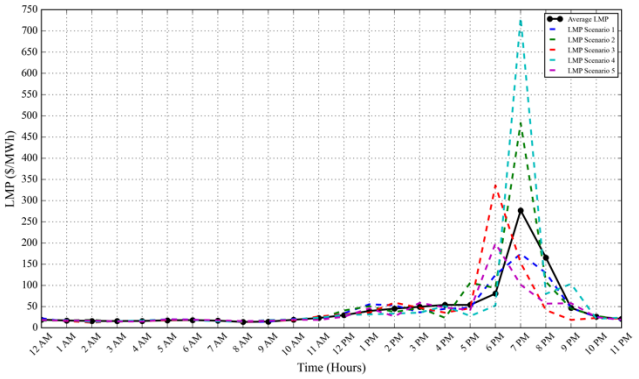

Figure 2. The electricity market prices (in $/MWh) of the five scenarios considered.

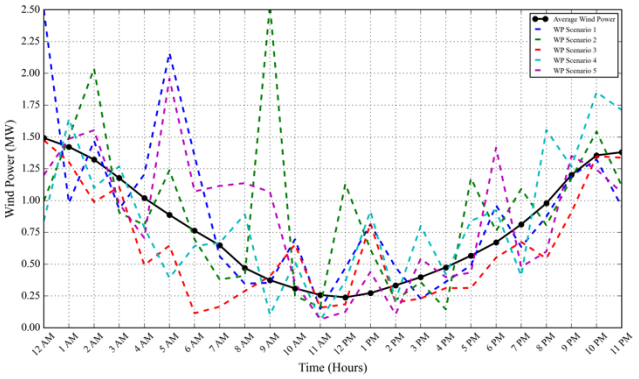

Figure 3. The generation output (in MW) of wind turbines of the five scenarios considered.

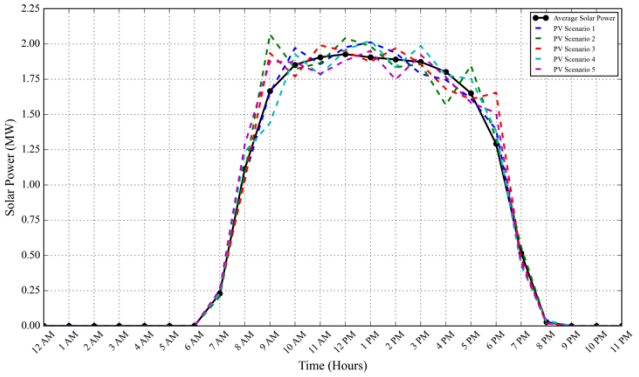

Figure 4. The output power (in MW) of solar panels of the five scenarios considered.

First, we solve the problem without incorporating the ϵ -constraint of Equation (2) to determine the

minimum operating cost and the corresponding degree of electrification (i.e., % of ethylene produced from ECs) required. The minimum expected daily operating cost is calculated to be $11,705.22, with 5.28% of the daily ethylene production coming from electrified crackers. The expected daily CO_2-equivalent emissions amounted to 919.42 tons, with the maximum hourly emissions reaching 39.43 tons (the first row in **Table 3**).

Next, we solve the problem for different values of $\epsilon \in [32,39]$ to evaluate the corresponding optimal operating and degree of electrification. It is important to note that the problem becomes infeasible when $\epsilon = 32$, indicating that reducing the hourly CO_2-equivalent emissions to less than 33 tons is not feasible with the current technology. The results, summarized in **Table 3**, show that the highest degree of electrification achievable is 19.25%, which corresponds to an operating cost of $33,884.81 – a 189.5% increase compared to the case without the ϵ-constraint (the first row in **Table 3**). On the other hand, the expected daily CO_2-equivalent emissions are reduced by 13.86% (almost 130 tons).

Table 3: Summary of expected operating costs, degrees of electrification, and CO_2-equivalent emissions for different values of ϵ, highlighting the trade-offs between emissions reduction and associated costs.

#	ϵ (tons)	Expected CO_2-equiv emissions (tons)	Degree of electrification (%)	Expected operating cost ($)
1	39	918.70	5.46	11,755.57
2	38	910.08	7.65	12,172.48
3	37	887.99	12.06	14,225.26
4	36	863.99	14.59	17,556.30
5	35	840.00	16.77	21,792.20
6	34	815.99	18.49	27,436.60
7	33	792.00	19.25	33,884.81

Here, we discuss some of the key findings and results. First, **Figures 5 and 6** illustrate the Pareto front and the operating cost-degree of the electrification relationship, respectively, providing quantitative insights into the trade-off between the two important measures. Meanwhile, **Figure 7 and 8** illustrate changes in the expected transferred power from the main grid to the microgrid and the charge/discharge status of local energy storage system (batteries). As one would expect, these fluctuations are partly driven by hourly variations in electricity market prices (as shown in **Figure 2**). During peak hours, there will be less power transferred from the main grid to the microgrid, thereby prompting the chemical plant to prioritize local power generation or stored energy to maintain continuous operation. During off-peak hours, the microgrid can rely more on the main grid power to reduce operating costs. Additionally, this figure highlights the environmental considerations affecting grid power usage. As stricter CO_2-equivalent emission constraint (ϵ) is enforced, the microgrid reduces its reliance on the main grid and favors cleaner, locally generated energy sources. This is due to the relatively high carbon footprint associated with main grid electricity given the existing energy landscape. Therefore, decarbonization of chemical manufacturing should not be considered in silo. Instead, it must be synergistically coupled with decarbonization in power systems to achieve holistic decarbonization that is economically favorable.

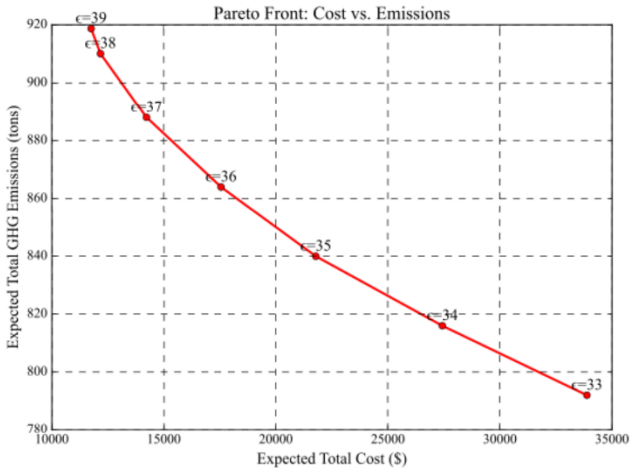

Figure 5. Pareto front showing the trade-off between expected daily operating cost and expected daily CO_2-equivalent emissions for different values of ϵ. Each point represents an optimal solution for a specific ϵ-value.

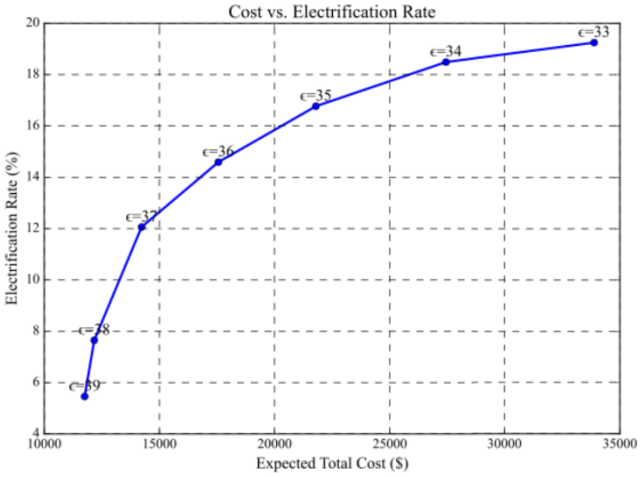

Figure 6. A concave relationship between expected operating cost and degree of electrification for different values of ϵ. The plot highlights how the tightness of emission constraint affects of optimal degree of electrification and cost.

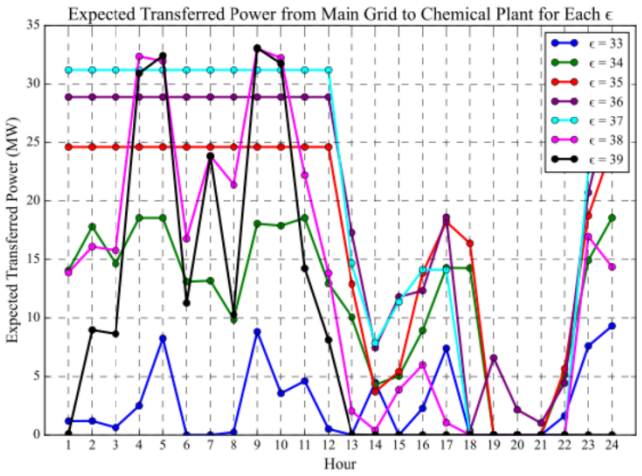

Figure 7. Expected transferred power from the main grid to the chemical plant.

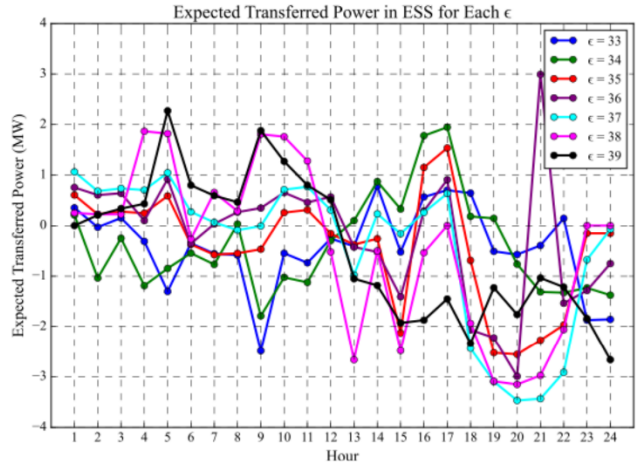

Figure 8. Expected charge/discharge power from ESS to ECs.

CONCLUSION

This work presents an optimization framework for operating the microgrid that integrates electrified and conventional steam crackers along with renewable energy sources and diverse energy sources and storage systems. The proposed multi-objective scenario-based MILP model illustrates the feasibility of reducing CO2-equivalent emissions and the resulting process economics trade-off. The results suggest that, while higher degree of electrification leads to lower emissions, there is a lower limit to which electrification and decarbonization of steam cracking process can reach given 1) the limited capacities of energy storage systems and technology readiness of fuel cells and electrolyzers, and 2) the resulting increase in operating cost. Overall, operating the ethylene plant as a microgrid offers flexibility and resilience as it can better cope with the ongoing industrial decarbonization initiatives and the evolving U.S. energy landscape. Our proposed microgrid superstructure provides a viable solution for energy-intensive steam cracking process to transition toward being sustainable while economically competitive. Looking ahead, further research should explore the integration of emerging energy storage technologies, such as advanced batteries and thermal storage, to enhance the stability of electrified steam cracking. Additionally, policy incentives and carbon pricing mechanisms could play a critical role in making sustainable production pathways more economically viable. Future studies should also investigate the electrification of other key process units, such as distillation systems using heat pumps, and assess the feasibility of fully electrified cracking plant. Addressing these aspects will unlock the full decarbonization potential of clean olefins production while ensuring operational reliability and economic feasibility.

ACKNOWLEDGEMENTS

This work is supported by the U.S. National Science Foundation under Award 2343072.

REFERENCES

1. U.S. EIA. Annual Energy Outlook 2022. (2022)
2. T. Sinn, M. Hofstaetter, R. Kemper, and G. Kracker, Powering the Transition to Net Zero with Electric Cracking Technology. Chem. Eng. Prog. 120:42-49. (2024)
3. R. Agrawal, Z. Chen, and P. Oladipupo. Electrically heated dehydrogenation process. U.S. Patent Application: 2021395170-A1 (2021)
4. D. Maporti, F. Galli, P. Mocellin, and G. Pauletto. Flexible ethylene production: Electrified ethane cracking coupled with oxidative dehydrogenation. Eng Conversion and Management, 298:117761. (2023)
5. S. Du, Z. Chen, and R. Agrawal. Assessing large energy storage requirements for chemical plants powered with solar and/or wind electricity. Chem. Eng. J. 505:158863. (2024)
6. R. Agrawal and J. Siirola. Decarbonization of chemical process industries via electrification. (2023)
7. S. Ghasemi Naraghi, T. Kareck, R. Reed, P. Ramanan, and Z. Jiang. Decarbonization of Steam Cracking for Clean Olefins Production: Microgrid Planning and Operation. In: Optimization of Sustainable Process Systems: Multiscale Models and Uncertainties. John Wiley & Sons, Inc. (2025)
8. D. T. Ton and M. A. Smith. The U.S. department of energy's microgrid initiative. The Electricity Journal 25:84–94. (2012)
9. A. Khodaei. Microgrid optimal scheduling with multi-period islanding constraints. IEEE Transactions on Power Systems 29:1383–1392.

(2013)
10. A. G. Tsikalakis and N. D. Hatziargyrio. Centralized control for optimizing microgrids operation. IEEE power and energy society general meeting 1–8. (2011)
11. A. Gholami, T. Shekari, F. Aminifar, and M. Shahidehpour. Microgrid scheduling with uncertainty: The quest for resilience. IEEE Transactions on Smart Grid 7:2849–2858. (2016)
12. Tesla. Industrial lithium-ion battery emergency response guide. (2022)
13. A. Elmouatamid, R. Ouladsine, M. Bakhouya, N. El Kamoun, M. Khaidar, and K. ZineDine. Review of control and energy management approaches in micro-grid systems. Energies 14:168. (2020)
14. U.S EIA. Carbon dioxide emissions coefficients. https://www.eia.gov/environment/emissions/co2_vol_mass.php. (2024)
15. U.S EPA. Greenhouse gas equivalences calculator. https://www.epa.gov/energy/greenhouse-gas-equivalencies-calculator-calculations-and-references. (2022)
16. M.S. Yancheshmeh, S.S. Haghighi, M. Gholipour, O. Dehghani, M. Rahimpour, and S. Raeissi. Modeling of ethane pyrolysis process: A study on effects of steam and carbon dioxide on ethylene and hydrogen productions. Chem. Eng. J. 215:550. (2013)
17. B. Nicholson, J. Siirola, J.-P. Watson, V. Zavala, and L. Biegler. pyomo.dae: a modeling and automatic discretization framework for optimization with differential and algebraic equations. Mathematical Programming Computation, 10:187. (2018)
18. D.-Y. Lee and A. Elgowainy. By-product hydrogen from steam cracking of natural gas liquids (NGLs): Potential for large-scale hydrogen fuel production, life-cycle air emissions reduction, and economic benefit. International Journal of Hydrogen Energy 43:20143–20160. (2018)
19. U.S. DOE. Renewable electrolysis integrated systems development and testing. (2016)